# Diffraction of polar molecules at nanomasks with low charge density

Ksenija Simonović,[1,*] Richard Ferstl,[1] Anders Barlow,[2] Armin Shayeghi,[1,3] Christian Brand,[4] and Markus Arndt[1,†]

[1]*University of Vienna, Faculty of Physics, VDS, VCQ, Boltzmanngasse 5, A-1090 Vienna, Austria*

[2]*University of Melbourne, Faculty of Engineering and Information Technology, Materials Characterisation and Fabrication Platform, Grattan Street, Parkville, Victoria 3010, Australia*

[3]*Institute for Quantum Optics and Quantum Information, Boltzmanngasse 3, A-1090 Vienna, Austria*

[4]*German Aerospace Center (DLR), Institute of Quantum Technologies, Wilhelm-Runge-Straße 10, 89081 Ulm, Germany*

(Received 11 January 2024; accepted 8 July 2024; published 25 July 2024)

The wave nature of matter is a cornerstone of modern physics and has been demonstrated for a wide range of fundamental and composite particles. While diffraction at nanomechanical masks is usually regarded to be independent of internal atomic or molecular states, the particles' polarizabilities and dipole moments lead to dispersive interactions with the grating surface. In prior experiments, such forces largely prevented coherent diffraction of polar molecules as they induce dephasing of the matter wave in the presence of randomly distributed charges inside the grating. Here, we show that surface milling using neon ions facilitates the fabrication of lowly charged nanomasks in gold-capped silicon nitride membranes. This allows us to observe diffraction of polar molecules with over four times larger electric dipole moment than in previous experiments, opening a path towards distinction of structural conformers in matter-wave experiments.

DOI: 10.1103/PhysRevResearch.6.033109

## I. INTRODUCTION

Advances in the machining of nanomechanical transmission masks have led to a multitude of optical elements for matter waves. These include slits, gratings, zone plates, and holograms for electrons [1–3], neutrons [4], atoms, and molecules [5–13]. Diffraction at nanomechanical gratings was the key to proving the existence of the helium dimer [14] and in the first demonstration of the wave nature of hot $C_{60}$ fullerenes [12]. Nanomechanical masks have been successfully employed in full-fledged matter-wave interferometers across a mass range spanning seven orders of magnitude [15–20]. This wide applicability stems from the fact that nanogratings modulate the wavefront of the incident matter wave. In first approximation, this effect is independent of any internal particle property, and nanomechanical gratings are hence considered to be "universal."

For applications in electron interferometry, however, the nanogratings must be conductive to prevent decoherence due to random potentials caused by trapped charges [17,21]. Atoms and molecules, on the other hand, are affected by the dispersive Casimir-Polder interaction [22–24]. This conservative potential attracts the particles towards the grating walls, thus populating higher diffraction orders than one would expect based solely on the geometrical slit width. In the case of highly polarizable macromolecules, the attraction becomes so pronounced that it may even require substituting mechanical gratings by optical ones [25,26]. To mitigate this effect, gratings have been thinned down to the level of single-layer graphene [27]. Nevertheless, even in thin membranes ion beam writing can implant ions or alter the material, which causes additional interactions [28–30]. These might exceed the Casimir-Polder interaction by an order of magnitude, thus dominating the interaction while the particle traverses the grating [28]. The ensuing phase shift depends on the molecular geometry, the velocity, internal degrees of freedom, and in particular the charge distribution inside the molecule and the membrane [31,32]. Even though matter-wave diffraction is about the center-of-mass motion of particles, dephasing associated with the orientation of polar molecules close to nanomechanical masks can suppress the observation of interference [32].

In our present paper, we push the development of nanomasks to create gratings that are compatible with the coherent diffraction of molecules with electric dipole moments beyond 8 D. This is achieved by employing neon ion beam milling, which deposits less charges in the material than the more common gallium ion beam writing. In addition, we apply a thin gold coating onto the insulating silicon nitride membranes before the milling step. Because of their increased versatility, the masks presented here allow us to derive useful information about the structure and bond configurations of molecules in the gas phase. We exemplify this in the analysis of 6,11-dihydroxy-5,12-naphthacenedione, where we can differentiate between conformational isomers using matter-wave diffraction.

*Contact author: ksenija.simonovic@univie.ac.at

†Contact author: markus.arndt@univie.ac.at

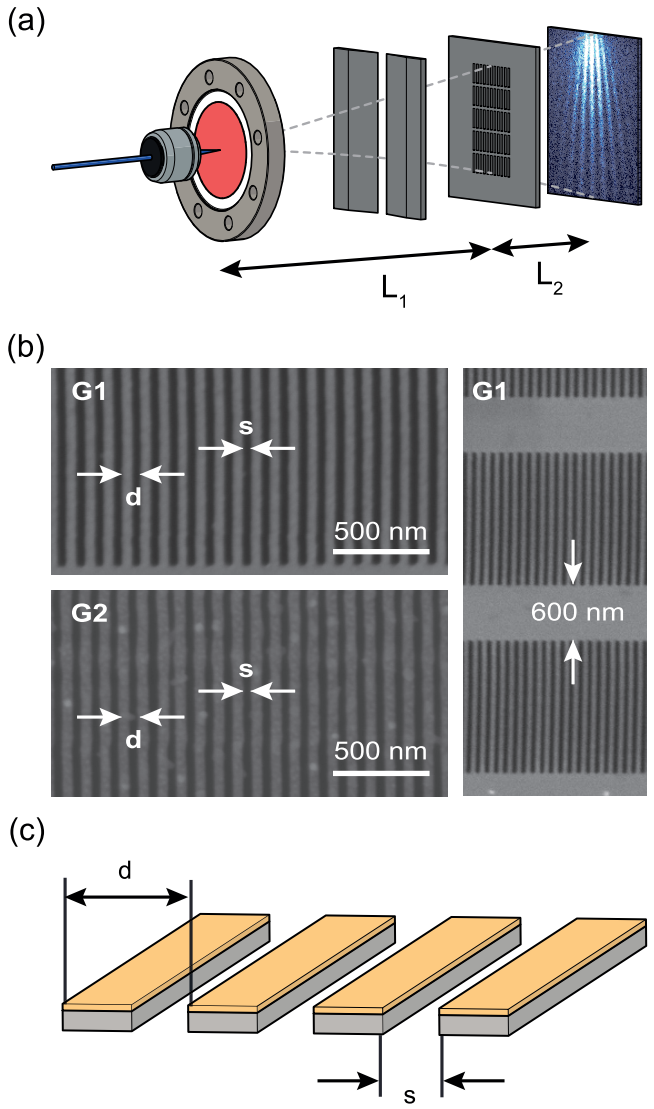


FIG. 1. (a) Experimental setup: Molecules are sublimated by a microfocused laser beam and collimated horizontally to below 3 μrad before being diffracted at a nanomechanical grating. The diffraction pattern is collected on a quartz window and imaged using fluorescence microscopy. (b) Scanning electron micrographs of gratings G1 (20-nm thickness) and G2 (55-nm thickness) illustrating the period $d$ and the slit width $s$. The zoomed-out view on the right of G1 shows the 600-nm high horizontal support bars. (c) Nanomechanical grating illustrating the 5-nm thin gold coating on top of the $SiN_x$ membrane.

## II. EXPERIMENTAL SETUP

Our experiment is based on earlier work [33] and sketched in Fig. 1(a). We coat a thin film of molecules onto the inside of a vacuum window and evaporate it with a laser beam at $\lambda = 421$ nm, focused to a spot size below 5 μm. The emergent molecular beam is collimated by a vertical slit to a divergence angle smaller than 3 μrad before it reaches the diffraction grating at $L_1 = 0.91$ m behind the source. About $L_2 = 0.70$ m behind the grating the diffraction pattern is captured on a 170-μm-thick quartz slide, which closes the vacuum chamber. The molecular pattern is detected and imaged using wide-field laser-induced fluorescence microscopy.

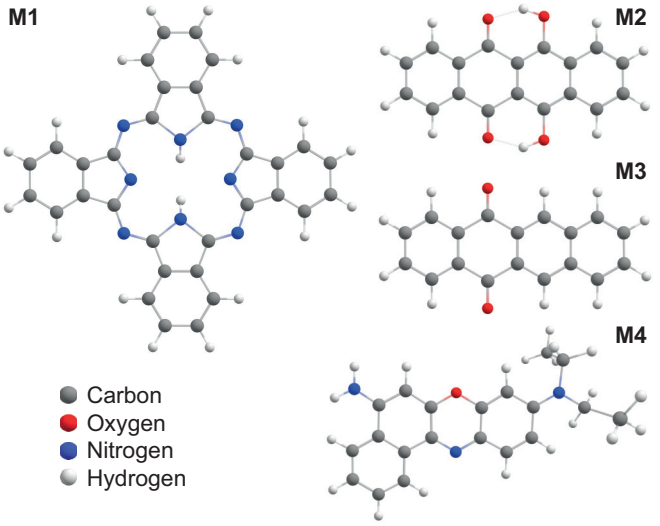


FIG. 2. Molecular structures of the systems used in this study: phthalocyanine (M1), 6,11-dihydroxy-5,12-naphthacenedione (M2), 5,12-naphthacenequinone (M3), and Nile red (M4).

Gratings in previous matter-wave diffraction experiments were manufactured using electron beam writing [5], photolithography [37], or focused gallium ion beam writing (Ga-FIB) [33]. Here, we use a focused beam of neon ions (Ne-FIB) to mill the gratings into two different silicon nitride membranes ($SiN_x$, Ted Pella) with a thickness of 15 and 50 nm, respectively. Both membranes were coated with a 5-nm thin gold layer on one side to neutralize implanted charges and to shield electric fields [see Fig. 1(c)]. The writing was done on an Orion NanoFab system (Zeiss, Germany) using the NPVE software package (Fibics Inc., Canada). We used an ion energy of 25 keV and an ion current of about 10 pA with a 20-μm beam defining aperture for a source pressure of neon of $5 \times 10^{-6}$ Torr. The dwell time for both patterns was 5 μs, with a dose of 0.1 nC/μm$^2$.

The resulting gratings are shown in Fig. 1(b). To ascertain the grating parameters, the images were converted to grayscale, vertically integrated, and normalized. The minima in these image traces correspond to the slits in the grating. An array of Gaussian functions was fitted to these minima to extract the grating period $d$. The geometrical slit width $s$ is the full width at half maximum of these Gaussian peaks. The grating G1 is $t = 20$ nm thick with a $d = 97(2)$ nm period and slit width $s = 46(2)$ nm. For G2 the parameters are $t = 55$ nm, $d = 99(2)$ nm, and $s = 43(2)$ nm. In both cases, the uncertainties are limited by the resolution of the electron microscope imaging. The structure is additionally stabilized by 600-nm-wide horizontal support bars [see Fig. 1(b)]. Note that, even though we present two specific gratings here, several gratings were written in similar membranes yielding consistent results.

To explore the compatibility of the gratings with coherent diffraction of polar particles, we compare the patterns of the four molecules shown in Fig. 2. These are phthalocyanine (M1), 6,11-dihydroxy-5,12-naphthacenedione (M2), 5,12-naphthacenequinone (M3), and Nile red (M4) with their molecular parameters shown in Table I. In this paper, especially the magnitude of the electric dipole moment

TABLE I. Properties of molecules used in the experiment: chemical formulas, mass, and permanent electric dipole moment. The listed dipole moments refer to experimentally obtained values unless otherwise specified. The two values for M4 have been obtained using solvatochromic and thermochromic studies respectively and hence vary slightly [36]. We use the higher value of 8.9 D throughout the paper.

| Label | Formula | Mass (u) | Dipole moment (D) |
|---|---|---|---|
| M1 | $C_{32}H_{18}N_8$ | 514.54 | 0.0 [34] |
| M2 | $C_{18}H_{10}O_4$ | 290.27 | 0.4 (see Fig. 4) |
| M3 | $C_{18}H_{10}O_2$ | 258.27 | 0.9 (calc.)/2.3 (expt.) [35] |
| M4 | $C_{20}H_{18}N_2O_2$ | 318.38 | 8.4–8.9 [36] |

is relevant, which varies between zero for phthalocyanine and 8.9 D for Nile red. For the different ground state geometries of M2 these were computed using density functional theory within the GAUSSIAN 16 program package. We used the LC-$\omega$PBEh functional [38] together with the def2tzvpp basis set [39,40]. The fluorescence excitation wavelengths ($\lambda_{M1} = 661$ nm, $\lambda_{M2,M3} = 421$ nm, $\lambda_{M4} = 532$ nm) and imaging bandpass filters ($\lambda_{M1} = 711/25$ nm, $\lambda_{M2,M3} = 550/88$ nm, $\lambda_{M4} > 550$ nm) were chosen to match the respective absorption and emission spectra.

## III. RESULTS AND DISCUSSION

Diffraction of the nonpolar molecule phthalocyanine (M1) at the 20-nm grating G1 leads to well-resolved diffraction peaks up to the fifth order, as shown in Fig. 3(a). For the 55-nm grating, we observe no significant changes in the population of higher diffraction orders [Fig. 3(i)]. To compare the interaction strength of a molecule with different gratings, we fit the diffraction patterns with a textbook diffraction formula using a reduced effective slit width $s_{\mathrm{eff}}$. It mimics the population of higher diffraction orders due to attractive interactions by reducing the width of a noninteracting slit and was initially introduced in the context of helium diffraction [41]. This approach is motivated by the attractive forces deflecting molecules that traverse the grating close to the walls to beyond the range of the detection screen. Thus, only those parts of the wave function that pass close to the slit center will contribute to the final interference pattern. In our analysis, we consider only the grating interference fringes within the zeroth order peak of the single-slit diffraction pattern as higher orders fall below the noise level.

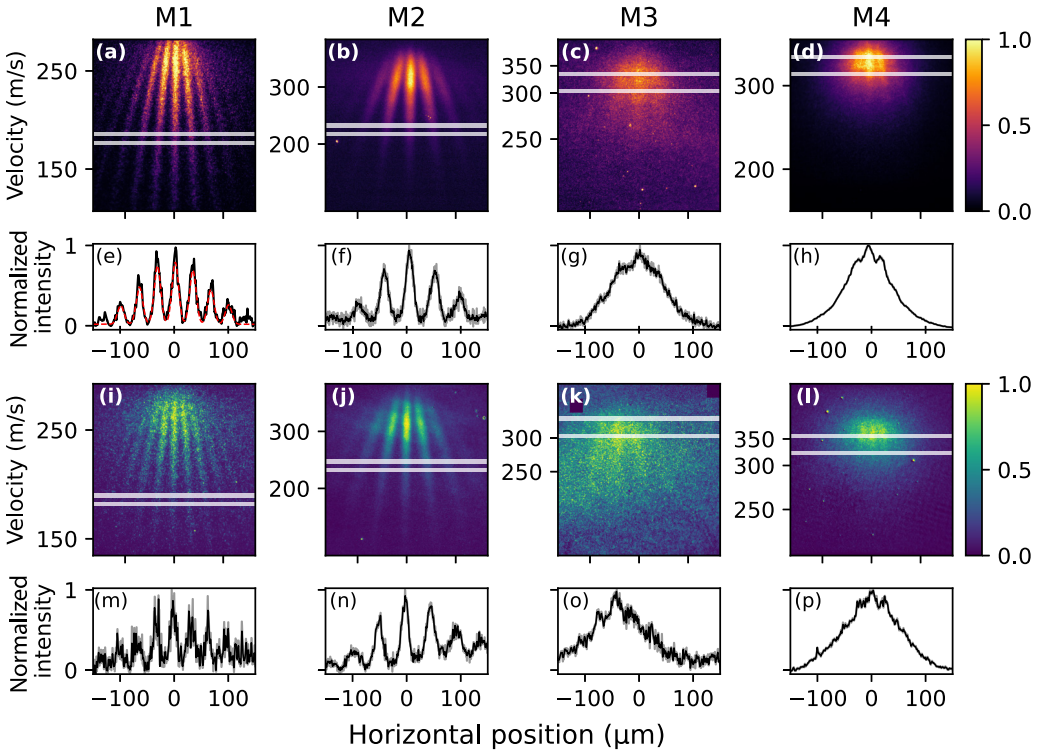


FIG. 3. [(a)–(d)] Normalized interference patterns behind the 20-nm thin grating. The molecules are sorted by their increasing electric dipole moment from left to right. The diffraction patterns are shown over a detector region of $300 \times 300\,\mu\mathrm{m}^2$. [(e)–(h)] Vertically binned and normalized traces of the regions enclosed by the white lines in the upper row. The light gray traces in the background are raw data; the black lines were smoothed using Savitzky-Golay filters for ease of view. The velocity bands were chosen for good contrast and good signal strength, centered around $\lambda_{\mathrm{dB}} = [4.3; 5.7; 4.8; 3.9] \times 10^{-12}$ m. The velocity scale for M3 and M4 is tentative because the peak separation and signal-to-noise ratio do not allow for an unequivocal assignment of $v$ over the whole image. All images are background corrected to account for illumination artifacts. [(i)–(p)] Same as upper two rows but for the 55-nm thin grating. The black squares in (k) block bright spots caused by contamination. In all panels, the $x$ scale is the same as on the screen in the laboratory. To convert it to diffraction angles in μrad, multiply the scale by 1.25 ($L_2 = 0.8$ m).

Theoretically more rigorous approaches describe the interaction, for instance, using Green's function and integrating over all forces along the molecular path [28,31]. In principle, this allows us to account for the attractive forces during the approach of the molecule towards the grating and geometrical details such as grating wedge angles. However, we decided against following this approach here, since this conceptually sophisticated model still needs to be complemented by a correction factor depending on the experimental details. In earlier studies, this factor was between 2 and 8, depending on the particle, the grating geometry and its deviations, and, most likely, the local charge distributions [28]. Luckily, and in contrast to earlier fabrication methods based on etching or Ga-FIB, neon FIB is known to produce nicer and steeper edges of milled structures [42], so that ignoring any potential wedge angles is a reasonable approximation.

For the 55-nm-thick grating G2 in our present experiments, the width of the Ne-FIB written slit is reduced from $s = 43$ nm to $s_{\mathrm{eff}} = 20$ nm, corresponding to a reduction factor $s/s_{\mathrm{eff}}$ of 2.2. This is significantly less than the factor of 3.3 observed in earlier experiments for M1 diffracted at a grating of comparable material and geometry (SiNx, $t = 45$ nm thick) but written with a focused gallium ion beam [27]. To test whether the reduction in the attractive interaction is due to fewer charges deposited in the material during the milling step, we have performed simulations using the software package SRIM [43]. We compare the implantation probability for gratings G1 and G2 considering both Ne ions at 25 keV as used here and Ga ions at 35 keV as used in previous realizations [33]. We simulate 10000 ion trajectories at normal incidence and compute the number of implanted ions by subtracting the transmitted and backscattered ions from the total amount. For $Ga^+$ at 35 keV, this results in implantation probabilities of 54.3 % for the thinner grating (G1) and 90.1 % for the thicker one (G2). In contrast to this, the probabilities are significantly lower for 25-keV Ne ions: 0.14 % for G1 and 0.76 % for G2. This decrease in implantation probability corroborates the assumption that the number of implanted charges in Ne-FIB milled gratings is overall lower, further motivating our method and justifying the interpretation. Increasing the grating thickness does not significantly influence $s_{\mathrm{eff}}$, again suggesting that the implanted charges are the dominant effect observed. The assumption is further supported by noting that both gratings were manufactured using identical Ne beam parameters. This is an important asset when the goal is to enable quantum diffraction of polar molecules at nanostructured masks.

The question now is how this improvement in the fabrication process affects the diffraction of polar molecules. In earlier experiments with gratings written via Ga-FIB in insulating $SiO_2$ membranes, the interference fringe contrast was already lost for molecules with a dipole moment of only 1.8 D [32]. Additionally, the membrane was ultrathin (8 nm) and the geometrical slit width $s$ amounted to 82 nm, substantially wider than in our present paper. In contrast to this, we still observe a finite interference contrast for Nile red (M4) diffracted at G1, even though its electric dipole moment of 8.9 D is more than four times larger than in the earlier studies [Fig. 3(d)]. In addition, we observe that increasing the thickness of the grating from 20 to 55 nm leads to similar results for all molecules, suggesting that the amount of implanted charges is small and comparable. While the SRIM-computed probability is higher for the thicker grating, both are well below 1 %, providing further evidence for this assumption.

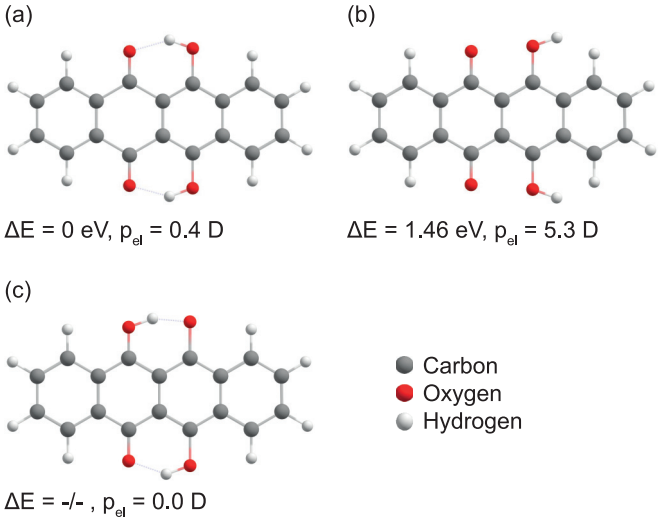


FIG. 4. Three conformation isomers of 6,11-dihydroxy-5,12-naphthacenedione, their relative energy $\Delta E$, and their ground state dipole moment $p_{\mathrm{el}}$. The absence of a dipole moment is indicative of a proton rapidly hopping or being shared between the oxygen atoms. While conformers [(a),(c)] are compatible with the matter-wave interference date, conformation (b) is experimentally clearly excluded.

### Impact of molecular geometry on diffraction pattern

Although dephasing due to local charges is considerably smaller in gratings written via Ne-FIB than in previous experiments [32], it is not entirely suppressed. Here we exploit this to make statements about the molecular geometries in the gas phase. As the loss of contrast is a function of the electric dipole moment, we can extract qualitative information about it from the observed matter-wave fringe contrast. We use this here specifically to study the structures of the two test molecules, 6,11-dihydroxy-5,12-naphthacenedione (M2) and naphthacenequinone (M3).

The two lowest-energy structures of M2, as obtained from our density functional theory calculations, are shown in Fig. 4. In Fig. 4(a) the OH groups are rotated toward the carbonyl groups, leading to an overall dipole moment of 0.4 D. In contrast to this, when both OH bonds are pointing away from the neighboring carbonyl groups, as shown in Fig. 4(b), the dipole moment increases by more than an order of magnitude to 5.3 D. In the experiment we find a high-contrast diffraction pattern for this molecule [Fig. 3(b)] which is only compatible with a small dipole moment, thus clearly excluding the possibility of the conformation isomer [Fig. 4(b)]. For the closely related molecule naphthazarin (M2 without the two outer hexagon rings) this conformational isomer is a stable minimum, lying 270 meV higher in energy than Fig. 4(a) [44]. However, even at a temperature of 800 °C in the source, the population of this conformational isomer is only on the order of a few percent. Hence, it is unlikely that it is responsible for the observed fringe pattern.

Another possibility is that the protons hop between the two binding sites on a timescale faster than the transit time of the molecule through the grating, effectively averaging out any possible dipole moment. In an aqueous solution, proton hopping is known to occur within 2 ps [45–47]. For M2 traveling at 300 m/s through the 20-nm-thick grating the transit time is 70 ps, which is long compared to the hopping time. Additionally, hopping may be facilitated by the internal molecular energy acquired during sublimation in the source.

For compound M3, one may expect an overall dipole moment close to zero, since the partial dipole moments of the two carbonyl groups seem to compensate each other. However, as shown in the third column of Fig. 3, the observed dephasing is much stronger than for M2. While earlier theoretical (0.87 D) and experimental works (2.3 D) differed [35], the observed dephasing points towards a dipole moment of at least 2 D, corroborating the prior experimental value. In all these experiments, one may speculate about the influence of molecular temperature. Thermally induced electric dipole moments have been observed in earlier matter-wave experiments with functionalized diazobenzenes, where they had a strong effect [48]. For phthalocyanine M1 the observation of high-contrast fringes indicates that it is too stiff to induce sizable thermal dipole moments. A similar geometric stability is predicted for the aromatic ring systems of M2 and M3. In Nile red (M4), the thermal contribution, however, is expected to be non-negligible.

In earlier matter-wave experiments, measurements of atomic polarizabilities [49,50] and molecular magnetism [51] were calibrated with specific atoms. It is tempting to propose the same for diffraction at our gratings employing diatomic molecules of well-known dipole moments as a reference. However, the molecule-wall interaction also depends on unknown parameters, such as excited rotational and vibrational states. This hampers an exact determination of the electric dipole moment. Nevertheless, the experiments allow us to estimate the magnitude, giving valuable insights into the molecular structure in the gas phase.

## IV. CONCLUSIONS

The fabrication of nanomechanical gratings using focused neon ion beams, capped with a thin gold layer, allowed us to observe interference of highly polar molecules at nanomechanical gratings. Such systems have until now inaccessible to matter-wave diffraction at mechanical masks. While dispersive forces close to the grating wall are often perceived as an obstacle to quantum experiments, we exploit them here to shed light on the internal structure of the molecules, mediated via their electric dipole moment. Grating diffraction is thus a surprisingly powerful tool to study aspects of molecular structure and physical chemistry. Interestingly, this information is accessible even while quantum delocalization prevents nature and the observer from knowing the exact location of the molecule in free flight. Comparing interference patterns of the same molecule behind different gratings should also provide information about surface charges implanted during the writing process or accumulated during the deposition process. Matter-wave diffraction of polar molecules is thus a sensitive tool to study charge effects.

Mechanical nanogratings will remain important for the manipulation of atoms and small molecules of low polarizability and low ionization yield and gratings with periods even below 50 nm seem to be in range. Such a tiny period cannot be achieved by optical diffraction gratings, and it would be relevant for the realization of two-dimensional diffraction masks for lightweight, fast, and polar molecules.

## ACKNOWLEDGMENTS

This research was funded in whole, or in part, by the Austrian Science Fund (FWF) [10.55776/DOC85] and [10.55776/P32543]. The work was in part conducted at the Materials Characterisation and Fabrication Platform at the University of Melbourne and the Victorian Node of the Australian National Fabrication Facility.

[1] G. Möllenstedt and C. Jönsson, Elektronen-mehrfachinterferenzen an regelmäßig hergestellten feinspalten, Z. Phys. **155**, 472 (1959).

[2] C. Jönsson, Electron diffraction at multiple slits, Am. J. Phys. **42**, 4 (1974).

[3] C. Jönsson, Elektroneninterferenzen an mehreren künstlich hergestellten Feinspalten, Z. Phys. **161**, 454 (1961).

[4] A. Zeilinger, R. Gähler, C. G. Shull, W. Treimer, and W. Mampe, Single- and double-slit diffraction of neutrons, Rev. Mod. Phys. **60**, 1067 (1988).

[5] D. W. Keith, M. L. Schattenburg, H. I. Smith, and D. E. Pritchard, Diffraction of atoms by a transmission grating, Phys. Rev. Lett. **61**, 1580 (1988).

[6] O. Carnal and J. Mlynek, Young's double-slit experiment with atoms: A simple atom interferometer, Phys. Rev. Lett. **66**, 2689 (1991).

[7] F. Shimizu, K. Shimizu, and H. Takuma, Double-slit interference with ultracold metastable neon atoms, Phys. Rev. A **46**, R17 (1992).

[8] J. Fujita, M. Morinaga, T. Kishimoto, M. Yasuda, S. Matsui, and F. Shimizu, Manipulation of an atomic beam by a computer-generated hologram, Nature (London) **380**, 691 (1996).

[9] R. B. Doak, R. E. Grisenti, S. Rehbein, G. Schmahl, J. P. Toennies, and Ch. Wöll, Towards realization of an atomic de Broglie microscope: Helium atom focusing using Fresnel zone plates, Phys. Rev. Lett. **83**, 4229 (1999).

[10] A. Luski, Y. Segev, R. David, O. Bitton, H. Nadler, A. R. Barnea, A. Gorlach, O. Cheshnovsky, I. Kaminer, and E. Narevicius, Vortex beams of atoms and molecules, Science **373**, 1105 (2021).

[11] M. S. Chapman, C. R. Ekstrom, T. D. Hammond, R. A. Rubenstein, J. Schmiedmayer, S. Wehinger, and D. E. Pritchard,

Optics and interferometry with $Na_2$ molecules, Phys. Rev. Lett. **74**, 4783 (1995).
[12] M. Arndt, O. Nairz, J. Vos-Andreae, C. Keller, G. van der Zouw, and A. Zeilinger, Wave-particle duality of $C_{60}$ molecules, Nature (London) **401**, 680 (1999).
[13] J. P. Cotter, C. Brand, C. Knobloch, Y. Lilach, O. Cheshnovsky, and M. Arndt, In search of multipath interference using large molecules, Sci. Adv. **3**, e1602478 (2017).
[14] W. Schöllkopf and J. P. Toennies, Nondestructive mass selection of small van der Waals clusters, Science **266**, 1345 (1994).
[15] D. W. Keith, C. R. Ekstrom, Q. A. Turchette, and D. E. Pritchard, An interferometer for atoms, Phys. Rev. Lett. **66**, 2693 (1991).
[16] G. van der Zouw and A. Zeilinger, Observation of the nondispersivity of scalar Aharonov-Bohm phase shifts by neutron interferometry, in *Epistemological and Experimental Perspectives on Quantum Physics*, Vienna Circle Institute Yearbook [1999], edited by D. Greenberger, W. L. Reiter, and A. Zeilinger (Springer, Dordrecht, 1999), pp. 263–265.
[17] G. Gronniger, B. Barwick, H. Batelaan, T. Savas, D. Pritchard, and A. Cronin, Electron diffraction from free-standing, metal-coated transmission gratings, Appl. Phys. Lett. **87**, 124104 (2005).
[18] B. Brezger, L. Hackermüller, S. Uttenthaler, J. Petschinka, M. Arndt, and A. Zeilinger, Matter-wave interferometer for large molecules, Phys. Rev. Lett. **88**, 100404 (2002).
[19] S. Sala, A. Ariga, A. Ereditato, R. Ferragut, M. Giammarchi, M. Leone, C. Pistillo, and P. Scampoli, First demonstration of antimatter wave interferometry, Sci. Adv. **5**, eaav7610 (2019).
[20] Y. Y. Fein, P. Geyer, P. Zwick, F. Kiałka, S. Pedalino, M. Mayor, S. Gerlich, and M. Arndt, Quantum superposition of molecules beyond 25 kDa, Nat. Phys. **15**, 1242 (2019).
[21] B. McMorran, J. D. Perreault, T. A. Savas, and A. Cronin, Diffraction of 0.5 keV electrons from free-standing transmission gratings, Ultramicroscopy **106**, 356 (2006).
[22] R. E. Grisenti, W. Schöllkopf, J. P. Toennies, G. C. Hegerfeldt, and T. Köhler, Determination of atom-surface van der Waals potentials from transmission-grating diffraction intensities, Phys. Rev. Lett. **83**, 1755 (1999).
[23] O. Nairz, M. Arndt, and A. Zeilinger, Quantum interference experiments with large molecules, Am. J. Phys. **71**, 319 (2003).
[24] C. Garcion, N. Fabre, H. Bricha, F. Perales, S. Scheel, M. Ducloy, and G. Dutier, Intermediate-range Casimir-Polder interaction probed by high-order slow atom diffraction, Phys. Rev. Lett. **127**, 170402 (2021).
[25] S. Gerlich, L. Hackermüller, K. Hornberger, A. Stibor, H. Ulbricht, M. Gring, F. Goldfarb, T. Savas, M. Müri, M. Mayor, and M. Arndt, A Kapitza-Dirac-Talbot-Lau interferometer for highly polarizable molecules, Nat. Phys. **3**, 711 (2007).
[26] O. Nairz, B. Brezger, M. Arndt, and A. Zeilinger, Diffraction of complex molecules by structures made of light, Phys. Rev. Lett. **87**, 160401 (2001).
[27] C. Brand, M. Sclafani, C. Knobloch, Y. Lilach, T. Juffmann, J. Kotakoski, C. Mangler, A. Winter, A. Turchanin, J. Meyer, O. Cheshnovsky, and M. Arndt, An atomically thin matter-wave beamsplitter, Nat. Nanotechnol. **10**, 845 (2015).
[28] C. Brand, J. Fiedler, T. Juffmann, M. Sclafani, C. Knobloch, S. Scheel, Y. Lilach, O. Cheshnovsky, and M. Arndt, A Green's function approach to modeling molecular diffraction in the limit of ultra-thin gratings, Ann. Phys. (Leipzig) **527**, 580 (2015).
[29] F. I. Allen, N. R. Velez, R. C. Thayer, N. H. Patel, M. A. Jones, G. F. Meyers, and A. M. Minor, Gallium, neon and helium focused ion beam milling of thin films demonstrated for polymeric materials: Study of implantation artifacts, Nanoscale **11**, 1403 (2019).
[30] C. Brand, M. R. A. Monazam, C. Mangler, Y. Lilach, O. Cheshnovsky, M. Arndt, and J. Kotakoski, The morphology of doubly-clamped graphene nanoribbons, 2D Mater. **8**, 025035 (2021).
[31] J. Fiedler and S. Scheel, Casimir-polder potentials on extended molecules, Ann. Phys. (Leipzig) **527**, 570 (2015).
[32] C. Knobloch, B. A. Stickler, C. Brand, M. Sclafani, Y. Lilach, T. Juffmann, O. Cheshnovsky, K. Hornberger, and M. Arndt, On the role of the electric dipole moment in the diffraction of biomolecules at nanomechanical gratings, Fortschr. Phys. **65**, 1600025 (2017).
[33] T. Juffmann, A. Milic, M. Müllneritsch, P. Asenbaum, A. Tsukernik, J. Tüxen, M. Mayor, O. Cheshnovsky, and M. Arndt, Real-time single-molecule imaging of quantum interference, Nat. Nanotechnol. **7**, 297 (2012).
[34] Y.-J. Yang, S.-X. Li, D.-L. Chen, and Z.-W. Long, Geometric structure, electronic, and spectral properties of metal-free phthalocyanine under the external electric fields, ACS Omega **7**, 41266 (2022).
[35] G. J. Gleicher, D. F. Church, and J. C. Arnold, Calculations on quinonoid compounds. II. Ground-state properties of quinones, J. Am. Chem. Soc. **96**, 2403 (1974).
[36] C. M. Golini, B. W. Williams, and J. B. Foresman, Further solvatochromic, thermochromic, and theoretical studies on Nile red, J. Fluoresc. **8**, 395 (1998).
[37] T. A. Savas, S. N. Shah, M. L. Schattenburg, J. M. Carter, and H. I. Smith, Achromatic interferometric lithography for 100-nm-period gratings and grids, J. Vac. Sci. Technol. B **13**, 2732 (1995).
[38] M. A. Rohrdanz, K. M. Martins, and J. M. Herbert, A long-range-corrected density functional that performs well for both ground-state properties and time-dependent density functional theory excitation energies, including charge-transfer excited states, J. Chem. Phys. **130**, 054112 (2009).
[39] F. Weigend, Accurate Coulomb-fitting basis sets for H to Rn, Phys. Chem. Chem. Phys. **8**, 1057 (2006).
[40] F. Weigend and R. Ahlrichs, Balanced basis sets of split valence, triple zeta valence and quadruple zeta valence quality for H to Rn: Design and assessment of accuracy, Phys. Chem. Chem. Phys. **7**, 3297 (2005).
[41] R. E. Grisenti, W. Schöllkopf, J. P. Toennies, G. C. Hegerfeldt, T. Köhler, and M. Stoll, Determination of the bond length and binding energy of the helium dimer by diffraction from a transmission grating, Phys. Rev. Lett. **85**, 2284 (2000).
[42] J. Sanz-Mateo, M. Deluca, B. Sartory, F. Benes, and D. Kiener, FIB and wedge polishing sample preparation for TEM analysis of sol-gel derived perovskite thin films, Ceramics **5**, 288 (2022).
[43] J. F. Ziegler, M. D. Ziegler, and J. P. Biersack, SRIM: The stopping and range of ions in matter (2010), Nucl. Instrum. Methods Phys. Res. B **268**, 1818 (2010).
[44] A. Jezierska, K. Błaziak, S. Klahm, A. Lüchow, and J. J. Panek, Non-covalent forces in naphthazarin: Cooperativity or competition in the light of theoretical approaches, Int. J. Mol. Sci. **22**, 8033 (2021).

[45] T. S. Light, S. Licht, A. C. Bevilacqua, and K. R. Morash, The fundamental conductivity and resistivity of water, Electrochem. Solid-State Lett. **8**, E16 (2004).

[46] S. Meiboom, Nuclear magnetic resonance study of the proton transfer in water, J. Chem. Phys. **34**, 375 (2004).

[47] R. Yuan, J. A. Napoli, C. Yan, O. Marsalek, T. E. Markland, and M. D. Fayer, Tracking aqueous proton transfer by two-dimensional infrared spectroscopy and *ab initio* molecular dynamics simulations, ACS Cent. Sci. **5**, 1269 (2019).

[48] M. Gring, S. Gerlich, S. Eibenberger, S. Nimmrichter, T. Berrada, M. Arndt, H. Ulbricht, K. Hornberger, M. Müri, M. Mayor, M. Böckmann, and N. L. Doltsinis, Influence of conformational molecular dynamics on matter wave interferometry, Phys. Rev. A **81**, 031604(R) (2010).

[49] W. F. Holmgren, M. C. Revelle, V. P. A. Lonij, and A. D. Cronin, Absolute and ratio measurements of the polarizability of Na, K, and Rb with an atom interferometer, Phys. Rev. A **81**, 053607 (2010).

[50] V. P. A. Lonij, C. E. Klauss, W. F. Holmgren, and A. D. Cronin, Atom diffraction reveals the impact of atomic core electrons on atom-surface potentials, Phys. Rev. Lett. **105**, 233202 (2010).

[51] Y. Y. Fein, S. Pedalino, A. Shayeghi, F. Kiałka, S. Gerlich, and M. Arndt, Nanoscale magnetism probed in a matter-wave interferometer, Phys. Rev. Lett. **129**, 123001 (2022).